Principal Curvature Ridges and Geometrically Salient Regions of Parametric B-Spline Surfaces

Suraj Musuvathy[a,*], Elaine Cohen[b], James Damon[c], Joon-Kyung Seong[d]

[a]*School of Computing, University of Utah*
[b]*School of Computing, University of Utah*
[c]*Department of Mathematics, University of North Carolina at Chapel Hill*
[d]*Korea Advanced Institute of Science and Technology*

Abstract

Ridges are characteristic curves of a surface that mark salient intrinsic features of its shape and are therefore valuable for shape matching, surface quality control, visualization and various other applications. Ridges are loci of points on a surface where one of the principal curvatures attain a critical value in its respective principal direction. We present a new algorithm for accurately extracting ridges on B-Spline surfaces and define a new type of salient region corresponding to major ridges that characterize geometrically significant regions on surfaces. Ridges exhibit complex behavior near umbilics on a surface, and may also pass through certain turning points causing added complexity for ridge computation. We present a new numerical tracing algorithm for extracting ridges that also accurately captures ridge behavior at umbilics and ridge turning points. The algorithm traverses ridge segments by detecting ridge points while advancing and sliding in principal directions on a surface in a novel manner, thereby computing connected curves of ridge points. The output of the algorithm is a set of curve segments, some or all of which, may be selected for other applications such as those mentioned above. The results of our technique are validated by comparison with results from previous research and with a brute-force domain sampling technique.

Keywords: ridge, parametric B-Spline surface, geometrically salient region

*Corresponding Author
Email addresses: srm@cs.utah.edu (Suraj Musuvathy), cohen@cs.utah.edu (Elaine Cohen), jndamon@math.unc.edu (James Damon), seong@kaist.ac.kr (Joon-Kyung Seong)

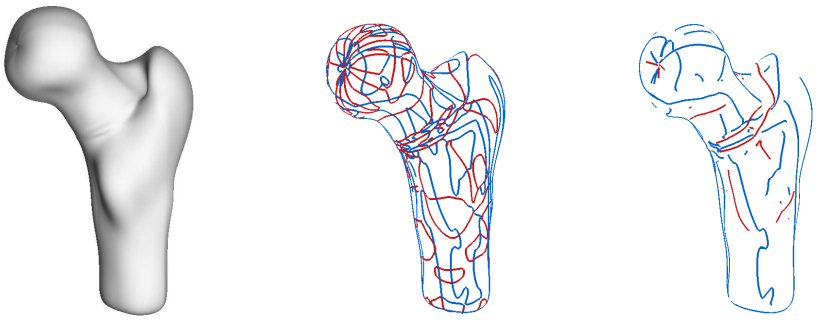

Figure 1: Ridges and crests of a femur B-Spline surface model.

1. Introduction

Ridge curves mark important intrinsic features of the shape of a surface. The formal mathematical study of the role of ridges in geometry began with the research of Porteous [1] and was first emphasized for shape analysis by Koenderink [2]. Since then, ridges have proven valuable in a variety of applications spanning diverse domains. They are view independent curves and more stable with surface deformation compared to other feature curves such as curvature lines, which makes them very useful for shape matching [3, 4, 5, 6]. They are useful in visualization applications since they capture perceptually salient features of an object [7, 8, 9]. Other applications include freeform surface quality control [10] and geophysical analysis [11, 12]. Figure 1 shows ridges and special types of ridges called crests of a B-Spline surface model of the upper part of a femur bone that have been computed using the technique presented in this paper.

A variety of approaches have been previously presented for computing ridges of discrete surface representations including polygonal meshes and images and implicit surface representations that are typically used to approximate discrete data. Estimating principal curvatures and their derivatives are major challenges for discrete surface representations. Tracing is relatively simpler and is typically performed by detecting crossings of ridges on the boundaries of mesh polygons or image voxels.

In contrast, principal curvatures and their derivatives can be computed exactly at specific points given a parametric surface representation with suf-

ficient smoothness, but tracing ridges is more difficult. In addition, ridges exhibit complex behavior around umbilics where multiple segments may coalesce, or form loops. Umbilics represent important features on surfaces and have been used in shape matching [13]. Therefore, it is essential to compute ridges around umbilics accurately. There are relatively few methods that address ridge computation at umbilics on parametric surfaces.

The main contribution of this paper is a new algorithm for computing ridges on tensor product B-Spline surfaces that also accurately captures ridge behavior at umbilics and other special points such as turning points. The algorithm traces ridges using localized curvilinear coordinate systems formed by principal curvature lines. Key results on computing principal curvature lines at umbilics, presented in [14], are utilized in the approach presented in this paper. The output of the algorithm is a set of ridge curve segments, that are available for use in other applications such as those mentioned previously. While the technique presented in this paper has been designed for tensor product piecewise rational parametric surfaces, it is quite general and extends to surface representations with multiple or trimmed patches with sufficient smoothness.

This paper also introduces a new type of geometrically salient region corresponding to major ridges. These salient regions also provide a means of measuring the importance of a ridge and its surrounding region in terms of higher order shape features. Earlier methods for quantifying the importance of ridges account for geometric properties only at ridge points [15, 16, 17]. The method introduced in this paper also considers salient neighborhood of ridges. Salient regions provide additional information for studying geometric variation of similar shapes and are especially useful when the ridges themselves do not provide sufficient information. For example, the location of the ridges may be very similar across a set of similar surfaces but the geometry of regions surrounding the ridges may vary. An example is presented in Section 8 to illustrate this situation.

1.1. Definition and Classification of Ridges

There are a number of different definitions of ridge curves on surfaces with different meaning and intent. We follow the notation given in [18, 19] and present that definition here. Consider a tensor product parametric surface $S(u, v) \in R^3$. Every point on $S(u, v)$, excluding umbilics, has two different principal curvatures ($\kappa_1 > \kappa_2$) and two corresponding principal

Table 1: Classification of Ridges

Ridge Type	Definition
κ_1-ridge	$\nabla_{t_1}\kappa_1 \stackrel{def}{=} \langle \nabla\kappa_1, t_1 \rangle = 0$
κ_2-ridge	$\nabla_{t_2}\kappa_2 \stackrel{def}{=} \langle \nabla\kappa_2, t_2 \rangle = 0$
Elliptic ridge	$\nabla_{t_1}\kappa_1 = 0, \quad t_1^T H_{\kappa_1} t_1 < 0$ $\nabla_{t_2}\kappa_2 = 0, \quad t_2^T H_{\kappa_2} t_2 > 0$ $H_{\kappa_i} = \begin{bmatrix} \kappa_{iuu} & \kappa_{iuv} \\ \kappa_{iuv} & \kappa_{ivv} \end{bmatrix}, i = 1, 2$
Crest (κ_2-crest $\rightarrow$ ravine or valley)	$\nabla_{t_1}\kappa_1 = 0, \quad t_1^T H_{\kappa_1} t_1 < 0, \quad \lvert\kappa_1\rvert > \lvert\kappa_2\rvert$ $\nabla_{t_2}\kappa_2 = 0, \quad t_2^T H_{\kappa_2} t_2 > 0, \quad \lvert\kappa_1\rvert < \lvert\kappa_2\rvert$

directions (t_1, t_2)[1]. Ridges are loci of points on a surface where one of the principal curvatures attains a critical value (i.e., local maximum, minimum or inflection) in its respective principal direction. This turns out to be equivalent to $\phi_i(u,v) = \langle \nabla \kappa_i, t_i \rangle = 0, i = 1$ or 2 (See [18, 20]). In this paper, we will henceforth refer to $\phi_i(u,v)$ as the *ridge condition* for the corresponding principal curvature.

Table 1 presents a classification of the various types of ridges. A ridge is called *elliptic* if κ_1 (κ_2) at a ridge point attains a local maximum (minimum) in the t_1 (t_2) direction, and termed *hyperbolic* otherwise. A *crest* is an elliptic ridge of the principal curvature with larger magnitude (See Table 1). The crest curve corresponding to the minimum principal curvature is typically called a *valley* or a *ravine*. It should be noted that some authors prefer to define ridges as the crest corresponding to the maximum principal curvature, while others refer to crests as κ_1-ridges, where $|\kappa_1| \geq |\kappa_2|$. In this paper, the term ridges encompasses crests, elliptic, and hyperbolic ridges.

1.2. Generic Properties of Ridges

Various aspects of the behavior of ridges on surfaces are summarized in this section (See [2, 18, 19, 21, 22] for discussions and proofs). In this paper, only the generic case is considered.

1. Two different ridges of the same principal curvature do not cross each other, except at umbilics. This property reduces the complexity of ridge tracing significantly.
2. κ_1-ridges may cross κ_2-ridges at so called *purple* points.
3. Ridges of a particular principal curvature do not have start or end points within a model (excluding the boundary of an open surface), except at umbilics.
4. Although principal directions are not defined at umbilics, ridges do occur at umbilics and exhibit complex behavior around umbilics.
5. Elliptic ridges, and therefore crests, do not occur at umbilics.
6. An umbilic may be classified as either a 1-ridge umbilic or a 3-ridge umbilic depending on the number of ridges arriving at the umbilic.
7. Ridges of a principal curvature intersect its corresponding principal direction transversally on the surface (R^3) except at a few isolated

[1] t_1 and t_2 are 2D vectors denoting elements of the tangent plane at $S(u,v)$.

locations. This property enables tracing ridges on local coordinate systems formed by principal directions on a surface.

8. Locations on the surface where a ridge is tangential to the corresponding principal direction are called *turning* points (also known as A_4 points in geometry and singularity theory). Turning points are detected using this property in the approach presented in this paper.
9. At a turning point, a ridge attains a local inflection in the corresponding principal direction and changes from being elliptic to hyperbolic or vice versa. This condition is given by $t_i^T H_{\kappa_i} t_i = 0, i = 1$ or 2. In this paper, this equation is not used since Property 8 allows identification of turning points without computing second order derivatives of curvatures.
10. A ridge of one principal curvature may be tangential to the other principal curvature direction on the surface (R^3) i.e., a κ_1-ridge may be tangential to the minimum curvature direction and vice versa. A good example is the equator of an ellipsoid.

This paper is organized as follows. Related research results on ridge computation are presented in Section 2. Section 3 presents background on differential geometry of surfaces. An overview of the ridge tracing algorithm is presented in Section 4 and the details are presented in Sections 5 and 6. Results and discussion on ridge computation are presented in Section 7. New results on identifying salient regions associated to major ridges are presented in Section 8, after which concluding remarks are made.

2. Previous Work on Extracting Ridges

Previous results on computing ridges of parametric surfaces can be classified into two categories: 1) direct computation of zero sets of the ridge condition equations, and 2) evaluation of the ridge condition on a tessellation of the parametric domain or other locations on a surface. The research presented in Cazals et al. [18, 21, 22] falls into the first category. In [18], a system of equations that encodes all the ridges and umbilics of a parametric surface represented by a single polynomial is presented. This system is essentially the product of the ridge conditions for both the principal curvatures. An algorithm is presented to solve the resulting polynomial equations using algebraic techniques [21, 22], and to compute topologically correct ridges. Their research presents the first technique to compute the topology of ridges

exactly at umbilics. Examples have been provided for single patch Bézier surfaces. The results computed using the technique presented in this paper are validated with an example from their research.

Other prior results for computing ridges on parametric surfaces fall into the second category. A method based on sampling the ridge condition on the curvature lines of a parametric surface and reporting a collection of points (without connectivity information) that satisfy the ridge condition (within some error criteria) is presented in Hosaka [10]. The notion of *crest bands* has been introduced in Jefferies [23]. Crest bands are *soft ridges* that satisfy the ridge condition within a given threshold at uniform samples in the parametric domain. This technique is also used for comparison and validation of the results presented in this paper. A similar approach for sampling the ridge condition on a regular rectangular grid in the parametric space of a surface represented by thin-plate splines and connecting neighboring ridge points on the grid has been presented in Guéziec [3]. Approximation of ridges on the edges of a triangulation of the parametric domain has been presented in Kent et al. [4] and Morris [24]. In the research presented by Morris [24], umbilics are first detected and ridge points are identified on circles surrounding the umbilics.

This paper presents a new approach based on numerically tracing zeros of the ridge condition within a user defined error bound, which may be arbitrarily small. Within the bounds of the numerical error, our technique accurately captures generic ridge behavior at all locations on a surface including umbilics. Our technique has been designed for rational B-Splines, which are used to represent complex surfaces in a rich variety of applications, and is reasonably fast for complex surfaces. For rational parametric surfaces (NURBS), the ridge equations have a very high degree, and hence, directly solving for the zero sets of the ridge condition is computationally expensive in terms of memory and processing time. In addition, to the best of our knowledge, there is no technique in the existing literature that can accurately compute the topology of ridges of NURBS surfaces at all locations from a disjoint set of ridge points. The authors of [21, 22] note that at the time of writing (2007), their technique for processing single polynomial surfaces was too slow to compute results in reasonable time for a bi-quintic Bézier patch. A domain tessellation or sampling-based method, albeit computationally fast, has other disadvantages. It is hard to obtain accurate ridges (exact zeros of the ridge condition) and connectivity information, especially at umbilics.

We briefly review some of the techniques used for computing ridges for

polygonal meshes, implicit surface representations and discrete images. This is by no means an exhaustive review, but enlists representative works in each area. For polygonal meshes, curvatures and their derivatives are approximated by a discrete differential geometry method [17, 25], by fitting a local or global smooth surface [15, 16, 26], or a combination of the two approaches [27]. The tracing methods typically follow vertices classified as ridge points or along the zero crossings of the ridge condition on the polygon edges. Geometric filtering approaches have been presented in Belyaev et al. [28] and Lai et al. [29]. For implicit surface representations, techniques for computing ridges via the intersection of the implicit surface and other implicit equations describing the ridges have been presented [30, 31, 32]. There has also been work on detecting ridges on images using nonlinear filtering techniques [28, 33]. Most of these techniques present results for only crest curves and thus, do not address ridges at umbilics.

3. Background

In this section, we review fundamental results on differential geometry that are utilized in this paper. For details, the reader is referred to [14, 34, 35].

3.1. Principal Curvatures and Principal Directions

Consider a regular tensor product parametric B-Spline surface $S(u, v) : [u^1, u^2] \times [v^1, v^2] \rightarrow R^3,\ S \in C^2$. The surface normal, $n(u, v) = \frac{S_u \times S_v}{||S_u \times S_v||}$ (assumed oriented inward for a closed surface, and $||S_u \times S_v|| \neq 0$ since S is regular) where, subscripts indicate the partial derivatives with respect to the corresponding parameter variable. The matrix of the first fundamental form of the surface is given by,

$$I = \begin{bmatrix} E & F \\ F & G \end{bmatrix} = \begin{bmatrix} \langle S_u, S_u \rangle & \langle S_u, S_v \rangle \\ \langle S_u, S_v \rangle & \langle S_v, S_v \rangle \end{bmatrix} \tag{3.1}$$

The matrix of the second fundamental form is given by,

$$II = \begin{bmatrix} L & M \\ M & N \end{bmatrix} = \begin{bmatrix} \langle S_{uu}, n \rangle & \langle S_{uv}, n \rangle \\ \langle S_{uv}, n \rangle & \langle S_{vv}, n \rangle \end{bmatrix} \tag{3.2}$$

Let A, B, C be defined as follows.

$$\begin{aligned} A &= EG - F^2 \\ B &= 2FM - GL - EN \\ C &= LN - M^2 \end{aligned} \tag{3.3}$$

Then, the principal curvatures at a point on the surface are given by,

$$\kappa_1 = \frac{-B + \sqrt{B^2 - 4AC}}{2A} \quad ; \quad \kappa_2 = \frac{-B - \sqrt{B^2 - 4AC}}{2A} \tag{3.4}$$

$$\kappa_1 \geq \kappa_2$$

κ_1 is termed the maximum principal curvature and κ_2 is termed the minimum principal curvature. The corresponding principal curvature directions are given by,

$$\begin{aligned} t_1 = \begin{bmatrix} t_1^1 \\ t_1^2 \end{bmatrix} = \begin{bmatrix} -(M - \kappa_1 F) \\ L - \kappa_1 E \end{bmatrix} \textit{ or } \begin{bmatrix} -(N - \kappa_1 G) \\ M - \kappa_1 F \end{bmatrix} \\ t_2 = \begin{bmatrix} t_2^1 \\ t_2^2 \end{bmatrix} = \begin{bmatrix} -(M - \kappa_2 F) \\ L - \kappa_2 E \end{bmatrix} \textit{ or } \begin{bmatrix} -(N - \kappa_2 G) \\ M - \kappa_2 F \end{bmatrix} \end{aligned} \tag{3.5}$$

The coefficients in the above equation are chosen so that the principal direction vectors are non-degenerate and as well-conditioned as possible. If only one of the vectors is well-conditioned, the following property enables computation of the other vector.

3.2. Orthogonal Property of Principal Directions

The vectors t_1 and t_2 lie in the tangent plane at $S(u, v)$ spanned by S_u and S_v. The model or Euclidean space vectors, denoted by T_1 and T_2 are given by,

$$\begin{aligned} T_1 = t_1^1 S_u + t_1^2 S_v \\ T_2 = t_2^1 S_u + t_2^2 S_v \end{aligned} \tag{3.6}$$

If $\kappa_1 \neq \kappa_2$, then $\langle T_1, T_2 \rangle = 0$, so the two principal directions are orthogonal at all non-umbilic points on the surface. (see lemma 12.47 of [34] or [35]). This property enables tracing ridges on a surface using local coordinate systems formed by T_1 and T_2 at non-umbilic points.

3.3. Three Types of Umbilics

Umbilics are points on the surface where the normal curvatures in all directions are equal. Therefore, $\kappa_1 = \kappa_2$ and the principal directions are not defined. However, lines of curvature exhibit three different patterns around

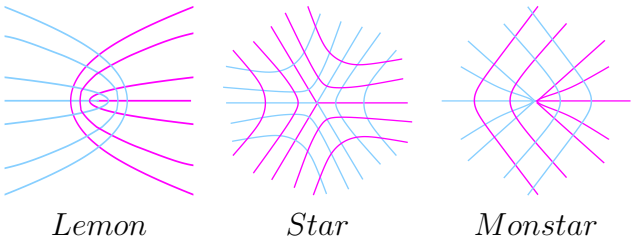

Figure 2: Patterns of principal curvature lines around umbilics. κ_1 curvature lines are indicated in pale blue and κ_2 curvature lines are in magenta.

generic umbilics denoted as the lemon, star, and (le)monstar patterns. Figure 2 shows the three different patterns formed by the principal curvature lines around umbilics[2]. At a lemon umbilic, there is a single principal direction that changes from being a maximum curvature principal direction to a minimum curvature principal direction. At a star umbilic, there are three such principal directions. A monstar umbilic is similar to a star umbilic, except that all maximum (minimum) curvature directions are contained within a right angle.

3.4. Principal Directions Around Umbilics

Maekawa and Patrikalakis [14, 36] presented a technique to distinguish between generic and non-generic umbilics and classify generic umbilics as lemon, star and monstar, and to compute exact principal direction patterns around umbilics. The principal directions were used in their work to trace curvature lines on a surface around umbilics. We employ this method to characterize behavior of ridges near umbilics. The idea is to represent the surface locally as a Monge patch in a reference frame centered at the umbilic and aligned with the tangent space of the surface at the umbilic. Then, the position vectors of the local maxima and minima of the Monge patch around the umbilic in the tangent space represent the maximum and minimum principal direction vectors. Details of this method can be found in [14]. Their approach also detects non-generic umbilics. We have not found any literature characterizing the behavior of principal curvature lines and ridges

[2]In geometry literature, blue and red colors have been used to indicate principal curvature lines as well as κ_1 and κ_2 ridges. In this paper, pale blue and magenta are used to depict curvature lines in order to distinguish between curvature lines and ridges.

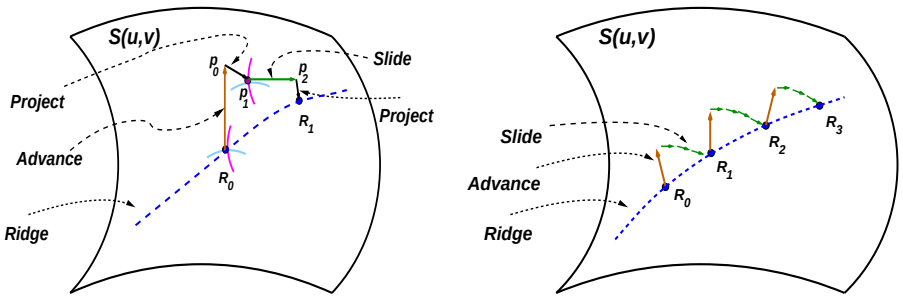

(a) Advance and slide steps for a single progress operation

(b) Several progress operations in a trace (projection steps not shown)

Figure 3: Tracing overview - advance and slide steps. Advance steps are shown in brown, projection operations are shown in black, slide steps are shown in green. Also shown are principal directions and ridges (dark blue).

around non-generic umbilics and hence chose not to address them in this paper.

At generic umbilics, there can either be a single maximum and minimum (lemon) or three maxima and minima (star and monstar). Maxima and minima occur on opposite sides of each other i.e., the angle between their position vectors is π. This phenomenon is shown in Figure 2, where the relevant maximum and minimum principal directions are opposite to each other.

4. Overview of Tracing Algorithm

The input surface, $S(u, v)$, is assumed to be regular (i.e., $S_u \times S_v \neq 0$), having only isolated umbilics, and ridges that exhibit only generic properties as specified in Section 1.2. The surface is also required to be C^3 smooth, in order to have continuous first order derivatives of principal curvatures. κ_1-ridges and κ_2-ridges are traced separately. In our discussion, we present the algorithm for tracing ridges corresponding to the maximum principal curvature (κ_1). The tracing procedure for κ_2-ridges is similar, and the differences are indicated at the end of the section after an overview of the algorithm has been presented.

Traces are started at various *seed points* including critical points of curvature and umbilics. Curvature critical points trivially satisfy the ridge condition since the curvature gradient is identically zero at these locations. Um-

bilics are also included as seed points since ridges may pass through these points.

Our strategy is based on the property that κ_1-ridges intersect the κ_1 curvature lines transversally except at a few isolated turning points. The idea is to trace a κ_1 curvature line to a zero of the ridge condition, where the κ_1 curvature line intersects a ridge. In order to progress to the next trace point, the algorithm steps along the κ_2 curvature line (T_2 direction) and then traces the κ_1 curvature line from the new location. Since the curvature lines are orthogonal, the algorithm is guaranteed to progress further along a ridge.

Each trace consists of several progress operations. Each progress operation consists of two steps viz., an *advance step*, and a *slide step*, as illustrated in Figure 3.

1. Advance step - compute a new point in the tangent plane of the current ridge point in the Euclidean minimum principal direction (T_2) and project it onto the surface.
2. Slide step - slide along the Euclidean maximum principal direction (T_1) and project onto the surface. Iterate until a zero of the ridge condition is reached (T_1 recomputed at each point).

Figure 3(a) shows an advance step and a slide that consists of a single step. In general, a slide may consist of several small sub-steps and the principal curvatures and directions are recomputed at every sub-step (Figure 3(b)).

The step sizes are varied adaptively (See Section 6). A trace ends when it reaches either another seed point or a parametric domain boundary. A new trace is also computed from the same seed point but by advancing in the opposite ($-T_2$) direction. Special care is needed when the trace is close to a turning point and when the trace is started at an umbilic. The following sections present details on computing seed points and the different tracing steps.

The algorithm for tracing κ_2-ridges differs in that the advance step is done along the maximum principal direction (T_1) and the slide step is performed along the minimum principal direction (T_2).

Away from umbilics, classical tracing methods via solutions of ordinary differential equations (ODEs) representing the ridges may be employed. However, such methods require higher order surface smoothness and are computationally more demanding since derivatives of the ridge condition are required. In our experiments, much smaller step sizes were required by the

ODE based method for achieving the same accuracy as the algorithm presented in this paper. In addition, singular points of the ridge condition are required for robust tracing via ODEs and the task of locating such points is computationally demanding due to the complexity of the ridge condition and its derivatives. Due to all the above reasons, the algorithm presented in this paper is computationally more suitable than ODE based methods for ridge tracing.

5. Computing Seed Points

This section presents systems of equations required to compute curvature critical points and umbilics based on [37, 14]. A robust and efficient subdivision-based constraint solving technique [38, 39] is used to compute the roots of relevant piecewise rational equations. The subdivision-based technique will compute all roots upto a user-specified tolerance [38].

5.1. Curvature Critical Points

Critical points of curvature occur at the locations on a surface where the curvature gradient is identically zero. Using the notation introduced in Section 3.1, and writing both principal curvatures in one equation,

$$\kappa(u,v) = \frac{-B \pm \sqrt{B^2 - 4AC}}{2A} \tag{5.1}$$

It is necessary to solve for simultaneous roots of

$$\begin{aligned} \kappa_u(u,v) &= 0, \\ \kappa_v(u,v) &= 0. \end{aligned} \tag{5.2}$$

$B(u,v)$ is not rational since it involves the coefficients of the second fundamental form, which in turn have a square root in the denominator. Noting that $||S_u \times S_v|| = \sqrt{A}$,

$$\begin{aligned} L = \frac{\widehat{L}}{\sqrt{A}}, \quad M = \frac{\widehat{M}}{\sqrt{A}}, \quad N = \frac{\widehat{N}}{\sqrt{A}} \\ B = \frac{\widehat{B}}{\sqrt{A}}, \quad C = \frac{\widehat{C}}{A} \\ \kappa(u,v) = \frac{-\widehat{B} \pm \sqrt{\widehat{B}^2 - 4A\widehat{C}}}{2A^{\frac{3}{2}}} \end{aligned} \tag{5.3}$$

where $\widehat{L}$, $\widehat{M}$, $\widehat{N}$, $\widehat{B}$, $\widehat{C}$ are piecewise polynomial or piecewise rational depending on whether $S(u,v)$ is piecewise polynomial or rational, respectively.

The first order derivatives of $\kappa(u,v)$ are given by,

$$\begin{aligned} \kappa_u &= P^{(u)} \pm \frac{R^{(u)}}{\sqrt{Q}} = 0 \\ \kappa_v &= P^{(v)} \pm \frac{R^{(v)}}{\sqrt{Q}} = 0 \end{aligned} \tag{5.4}$$

where,

$$\begin{aligned} P^{(u)} &= \tfrac{1}{2}[(-A^{\frac{-3}{2}}\widehat{B}_u + \tfrac{3}{2}A^{\frac{-5}{2}}A_u\widehat{B})] \\ P^{(v)} &= \tfrac{1}{2}[(-A^{\frac{-3}{2}}\widehat{B}_v + \tfrac{3}{2}A^{\frac{-5}{2}}A_v\widehat{B})] \\ R^{(u)} &= \tfrac{1}{2}[(A^{\frac{-3}{2}}\widehat{B}_u\widehat{B} - 2A^{\frac{-1}{2}}\widehat{C}_u + 4A^{\frac{-3}{2}}A_u\widehat{C} - \tfrac{3}{2}A^{\frac{-5}{2}}A_u\widehat{B}^2)] \\ R^{(v)} &= \tfrac{1}{2}[(A^{\frac{-3}{2}}\widehat{B}_v\widehat{B} - 2A^{\frac{-1}{2}}\widehat{C}_v + 4A^{\frac{-3}{2}}A_v\widehat{C} - \tfrac{3}{2}A^{\frac{-5}{2}}A_v\widehat{B}^2)] \\ Q &= \widehat{B}^2 - 4A\widehat{C} \end{aligned} \tag{5.5}$$

Note that,

$$\begin{aligned} \kappa_{1u} &= P^{(u)} + \frac{R^{(u)}}{\sqrt{Q}}, \quad \kappa_{1v} = P^{(v)} + \frac{R^{(v)}}{\sqrt{Q}} \\ \kappa_{2u} &= P^{(u)} - \frac{R^{(u)}}{\sqrt{Q}}, \quad \kappa_{2v} = P^{(v)} - \frac{R^{(v)}}{\sqrt{Q}} \end{aligned} \tag{5.6}$$

Moving the terms with the square root in Equation 5.4 to the right hand side, squaring both sides and simplifying we get,

$$\begin{aligned} QP^{(u)2} - R^{(u)2} &= 0 \\ QP^{(v)2} - R^{(v)2} &= 0 \end{aligned} \tag{5.7}$$

The above equations encode the critical points of both κ_1 and κ_2. After solving for the roots of the above system of equations, they are classified as critical points of κ_1 or κ_2 by evaluating Equation 5.6.

5.2. Umbilics

At umbilics, $\kappa_1 = \kappa_2$. Therefore, from Equation 5.3 it is apparent that,

$$Q(u,v) = \widehat{B}^2 - 4A\widehat{C} = 0 \tag{5.8}$$

In addition, $Q(u,v)$ attains a minimum at the umbilic (since $Q(u,v) \geq 0$). Therefore, the roots of the following system of equations are computed.

$$\begin{aligned} \frac{\partial Q(u,v)}{\partial u} &= 2\widehat{B}\widehat{B}_u - 4A_u\widehat{C} - 4A\widehat{C}_u = 0 \\ \frac{\partial Q(u,v)}{\partial v} &= 2\widehat{B}\widehat{B}_v - 4A_v\widehat{C} - 4A\widehat{C}_v = 0 \end{aligned} \tag{5.9}$$

Equation 5.8 is then evaluated to ensure $Q(u,v) = 0$ (since there may be local extrema of $Q(u,v)$ that do not occur at umbilics).

6. Tracing

As mentioned in Section 4, each trace consists of a series of advance and slide steps. For both these steps, consistent orientation of the principal directions and prudent step sizes must be chosen in order to successfully trace a ridge. We discuss each operation with respect to tracing a κ_1-ridge. The strategy for tracing at umbilics and the technique used for projecting points onto the surface at every step are also presented.

6.1. Advance Step

6.1.1. Orientation

At every advance step, it is necessary to ensure that the new T_2 vector is along the same direction as the previous T_2 vector and not opposite (by ensuring that the angle between the vectors in acute). The heuristic, called the acute angle rule [15], has been used for tracing ridges on polygonal meshes.

6.1.2. Step size

A judicious choice of step size is critical when two ridges are close. At every advance step, an initial step size δ_0 is first selected[3]. Let $r_i \in R^2$

[3]In our experiments, initial step sizes of 0.1% of the length of the diagonal of the bounding box of the surface worked well.

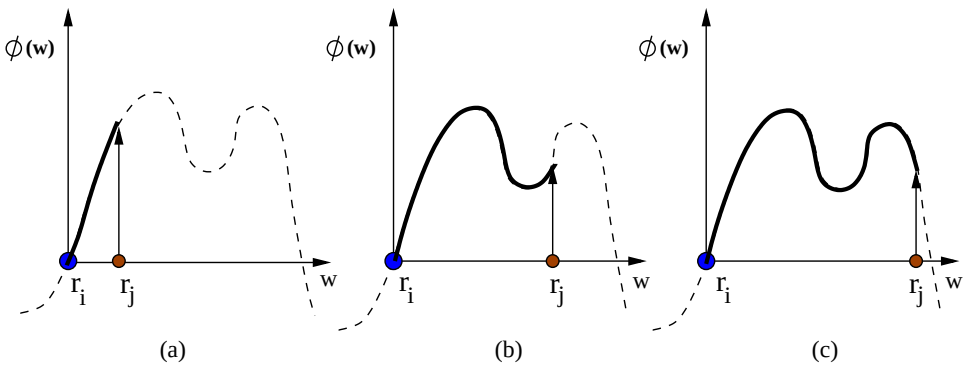

Figure 4: Robust initial advance step size selection. r_i is a ridge point and r_j is the advance point.The graph of $\phi(w)$ between r_i and r_j ($w \in [0,1]$) is shown as a thick curve. Broken curve segments indicate $\phi(w), w < 0, w > 1$. δ_0 should be chosen such that $\phi(w)$ does not have any local extrema between r_i and r_j. a) indicates a correct step size selection. b) and c) indicate incorrect step size selections. In case b), the trace will get stuck in a local minimum of $\phi(w)$ and will not reach a ridge. In case c), the trace will converge to an adjacent ridge segment.

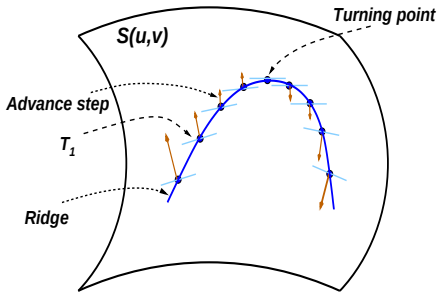

Figure 5: Advance step size (turning point aware). Advance steps are shown in brown, maximum curvature principal directions are shown in pale blue, ridge is shown in dark blue.

be the parameter values for the current ridge point and $r_j \in R^2$ be the parameter values for the point arrived at by advancing along the T_2 direction and projecting onto the surface. Let $\phi(u, v)$ represent the ridge condition for the current principal curvature. $\gamma(w) = (u(w), v(w)) = r_i + w(r_j - r_i), w \in [0, 1]$ is the line segment joining r_i and r_j. $\phi(\gamma(w))$ is the corresponding curve segment of the ridge condition between r_i and r_j. In order to guarantee robustness, the trace must not slide to either a local extremum of $\phi(u, v)$ or an adjacent ridge segment (See Figure 4). This condition can be enforced by ensuring that $\phi(\gamma(w))$ does not have any local extrema. The test would then involve checking whether or not the graph of $\phi(\gamma(w))$ has a zero slope at any point. However, computation of the slope requires higher order surface smoothness. In addition, $\phi(\gamma(w))$ is not a rational function. Therefore a computationally efficient approach similar to a Monte Carlo method requiring only samples of $\phi(\gamma(w))$ is used. The interval $w = [0, 1]$ is sampled randomly and $\phi(\gamma(w))$ is evaluated at the samples. The robustness test then checks if the samples of $\phi(\gamma(w))$ are monotonic with respect to w. δ_0 must be reduced until this condition is satisfied.

The advance step size is additionally varied adaptively during the trace depending on nearness to a turning point. The step size can be additionally scaled using curvature magnitude and curvature gradient magnitude at every step. Initially, at a seed point, there is no information about the ridge direction. From the next advance step onward the ridge direction is tracked using the previous trace points. The angle between the ridge direction and the T_1 direction computed at the current location is related to the proximity of a turning point. An angle close to zero implies that a turning point is very close. The step size is reduced accordingly during the trace until it falls below a threshold (`turning_point_stepsize_threshold`[4]). Once it falls below the threshold, the orientation of the T_2 vector is reversed since the ridge will now progress in the opposite direction. From the next advance step onward, the trace will use the new orientation of the T_2 vector. The ridge progress direction is used to avoid backtracking along the previously computed trace after a flip. The adaptive step size variation in the vicinity of a turning point is illustrated in Figure 5. Also, using a larger step size immediately after detecting a potential turning point and searching for a ridge by sliding from an advance step in both T_2 and $-T_2$ directions helps detect a geodesic

[4]We have used a threshold value of 10^{-6} in our experiments.

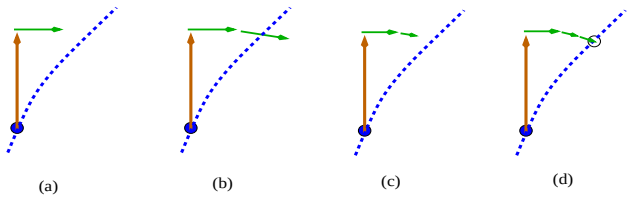

Figure 6: Sliding to a ridge. Advance step is shown in brown, slide steps are shown in green. a) First slide step is moving toward ridge but has not yet reached ridge, b) Second slide step has crossed ridge, c) Slide is recomputed with reduced step size, new slide point has not yet reached ridge, d) Slide has reached ridge after a few steps of b) and c).

inflection point of the ridge.

6.2. Slide Step

After an advance step is done, the slide begins with an initial step size and a local search is performed for a ridge in both T_1 and $-T_1$ directions. The technique presented in Section 6.1.2 can be used to ensure robust initial step size selection. Figure 6 shows a sample sliding scenario. The values of the ridge condition at the current location and a step from the current location in the T_1 direction are compared. If the ridge conditions at the two points have the same sign and have increasing magnitude, a slide is not performed in that direction. If they have the same sign and are decreasing in magnitude, the new location is accepted and the slide is repeated from the new location. If the signs are different (implying that the slide crossed a ridge), the slide step size is reduced[5] and a new location is recomputed from the current point along the T_1 direction at the current point. This process is repeated iteratively until the ridge condition falls below a specified threshold (`ridge_accuracy_threshold`)[6]. A local acute angle heuristic is used to select consistent T_1 vector orientations.

6.3. Tracing from Umbilics

The algorithm sweeps around umbilics using the principal curvature directions to detect ridges. If a ridge is found, a seed point is created and a trace is started in the direction away from the umbilic (See Figure 7 for illustration).

[5] In our experiments, we found that halving the step size works well.

[6] `ridge_accuracy_threshold` value of 10^{-3} was used in our experiments.

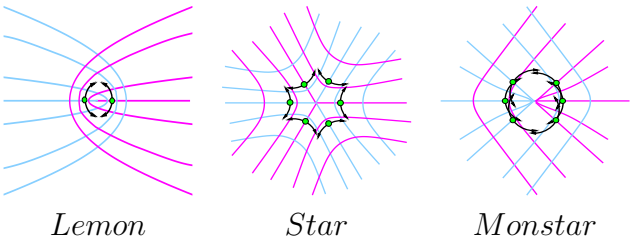

Figure 7: Tracing around umbilics. Scout points are shown in green.

Recall from Section 3.4 that there are either one or three pairs of minimum and maximum curvature directions oriented opposite each other. In any of these cases, a scout point is created at a small distance from the umbilic along each of the minimum curvature directions and traces are started from each of them as presented in the previous section. If the scout does not detect a ridge, it will stop automatically. If the scout does detect a trace, it will continue as if it were tracing from any other regular point. In addition, scout points are also created along the maximum principal directions in order to completely sweep around the umbilic.

It should be noted that it is possible to trace the same ridge multiple times (from start to end and reverse). At umbilics, a ridge can be traced multiple times from different seed points. Duplicate ridges are detected by inspecting the start and end points of the respective traces. In the latter case, the start points are the same umbilic point. In addition, the curvature lines may have a large geodesic curvature very close to an umbilic. The local acute angle rule may not guarantee consistent orientations in such cases, as noted by [15]. Therefore, to avoid such situations, the scout points must not be created too close to an umbilic. Tracing κ_2 ridges from umbilics is identical, since scout points are created in all principal directions.

6.4. Projecting Points onto Surface

At every step, when a motion is performed in either principal direction in the tangent plane of the surface, it is necessary to project the point onto the surface. In order to find the point on the surface $S(u, v)$ (and the corresponding parameter values) closest to a given point $X \in R^3$, a global approach involves solving the following system of equations.

$$\begin{aligned} \langle S_u(u,v), (S(u,v) - X) \rangle &= 0 \\ \langle S_v(u,v), (S(u,v) - X) \rangle &= 0 \end{aligned} \tag{6.1}$$

The solution set of this system of equations gives all points on the surface where the vector from the point X to a point on the surface is in the direction of the surface normal at that point. The actual closest point is determined by computing the distances from X to all the solutions and selecting the nearest one.

The global approach is too slow since the tracing algorithm may involve a very large number of projection operations. In this paper, a two dimensional Newton's method is used to find the closest point on the surface. This technique is very fast and has been used for interactive applications that require computing closest points at a very large rate (several hundred times a second) [40]. Since the step sizes used in the algorithm are typically very small, this works well. An alternative method presented in [41] can be used for point projection. In the event that the Newton's method fails to give accurate results, the algorithm reverts to the global method. In our experiments, this situation did not occur very often. The two dimensional Newton's method involves solving the following linear system of equations for variables u and v.

$$\begin{bmatrix} \frac{\partial(\langle S_u, Z\rangle)}{\partial u} & \frac{\partial(\langle S_u, Z\rangle)}{\partial v} \\ \frac{\partial(\langle S_v, Z\rangle)}{\partial u} & \frac{\partial(\langle S_v, Z\rangle)}{\partial v} \end{bmatrix} \begin{bmatrix} u - u_0 \\ v - v_0 \end{bmatrix} = - \begin{bmatrix} \langle S_u, Z\rangle \\ \langle S_v, Z\rangle \end{bmatrix} \tag{6.2}$$

$$Z = S - X$$

The Jacobian matrix can be expanded as,

$$\begin{bmatrix} \langle S_{uu}, Z\rangle + \langle S_u, S_u\rangle & \langle S_{uv}, Z\rangle + \langle S_u, S_v\rangle \\ \langle S_{uv}, Z\rangle + \langle S_u, S_v\rangle & \langle S_{vv}, Z\rangle + \langle S_v, S_v\rangle \end{bmatrix} \tag{6.3}$$

Symbolic representations of the partial derivatives of the surface are precomputed so that they can be evaluated quickly for the projection operations. The parameter values of the current advance or slide point are used as the initial point (u_0, v_0). This system is solved iteratively until the error is small enough. The error is computed as the residual from the evaluation of Equation 6.1.

7. Results on Ridge Computation and Discussion

The tracing algorithm has been implemented in the IRIT [42] programming environment. Experiments have been performed on an Intel 2.4GHz

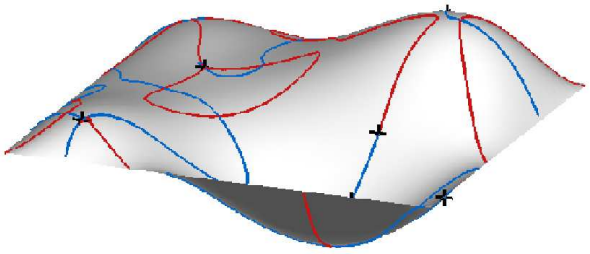

Figure 8: Ridges on a Bézier patch. κ_1-ridges are in blue and κ_2-ridges are in red.

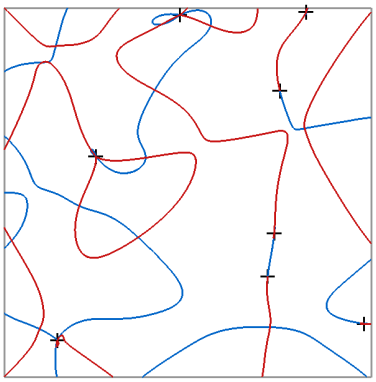

Figure 9: Ridges of Bézier patch depicted in parametric space. Black cross-hairs indicate umbilics.

processor with 8GB memory. We first present results for a simple bi-quartic Bézier patch (See Figures 8 and 9). This surface was selected to allow direct comparison with the results presented in [22] (See Figures 8.4 and 8.5 therein), which are topologically correct at all locations including umbilics. The results are best compared in parametric space. Figure 9 and Figure 8.4 of [22] are indeed very similar.

We also present ridges traced on complex models from different application domains including a human femur bone model and a terrain elevation map [43]. The surfaces are represented by tensor product bi-quartic B-Splines. The results are compared with a brute force sampling of the ridge condition in the parametric domain in Figures 10 and 11. Soft ridges, similar to the style presented in [23], are computed to present a better visualization. However, there is no topology associated with the sampled ridges. The images showing the sampled κ_1-ridges are colored with regions varying from blue fading into yellow. Images of the sampled κ_2-ridges are colored with regions varying from red fading into cyan. Darker blue colors in the former, and brighter red in the latter images correspond to regions closer to κ_1 and κ_2 ridges respectively.

The sampling approach can falsely indicate the presence (false positives) or absence (false negatives) of ridges. In Figure 12, the rectangular outline region shows an example where the presence of a κ_1-ridge is falsely indicated on the terrain elevation model. The κ_1 ridge samples indicate the presence of a ridge. However, a close inspection of the κ_2 ridge samples and the traced ridges indicate that there is a κ_2-ridge in that region, which is verified by the topology of the traced ridges in the surrounding region. False positives (+ve) occur when the magnitude of the ridge condition is small enough to pass a threshold used for coloring the samples, but not zero. Figure 12 also shows an example where the sampling approach fails to detect a κ_2-ridge (elliptic outline region) of the terrain elevation model, but is accurately captured using the tracing approach. False negatives(-ve) occur when width of the ridges is narrower (which can be arbitrarily narrow) than the sampling fineness. Figure 12.(b) shows that the tracing approach presented in this paper avoids the problems associated with sampling-based techniques and accurately captures ridge behavior.

While our algorithm is not designed for non-generic situations, end points of non-generic ridges that stop within the surface boundary are detected in our algorithm when the trace cannot detect any ridge during the slide step. Non-generic ridges of the same type may cross each other. The technique

presented here does not capture the topology at the junctions of ridges of the same type. This is an area for future work. Some non-generic ridge segments may be missed if the algorithm does not find seed points in those segments. Determining seed points that are neither curvature critical points nor umbilics to account for non-generic ridges is also an area for future work. However, since the curvature critical points and umbilics represent important feature points on a surface, the algorithm presented in this paper is guaranteed to capture salient ridges on a surface.

The constraint solver for computing seed points may give extraneous roots if too large a tolerance is allowed. These false roots will result in traces that end within a few steps, which is a non-generic situation. Such ridge traces are detected and removed.

Computational aspects for the different models on a single CPU are compared in Table 2[7]. The computation times vary depending on the complexity of the models, not only in terms of representation size, but also in terms of the features on the surfaces, on the accuracy of the ridge tracing and the average trace length. We used a `ridge_accuracy_threshold` of 10^{-3} for all data sets. The femur and the terrain models are quite complex, and our technique gives results in a few minutes. In comparison, an ODE based tracing method took several hours to compute ridges with the same accuracy. Since traces computed from different seed points are independent of each other, it is possible to perform them in parallel, which would further reduce computation time. The sampling method took 10 and 9 seconds for a 200 x 200 grid for the femur and terrain models respectively. However, as mentioned earlier, the sampled result does not provide accurate locations and topology of ridge points.

The technique presented in this paper requires C^3 surface smoothness. It is desirable to have similar techniques for surfaces with lower order smoothness. We are currently developing techniques to address this problem (See [44]). This research assumes surface regularity and the presence of only isolated generic umbilics. Addressing such situations is an area for future work.

8. Geometrically Significant Regions Associated with Ridges

Elliptic ridges (See Section 1.1) are identified in our work as major ridges and hyperbolic ridges are identified as secondary ridges. This section defines

[7]Time taken to create surface patches is not included.

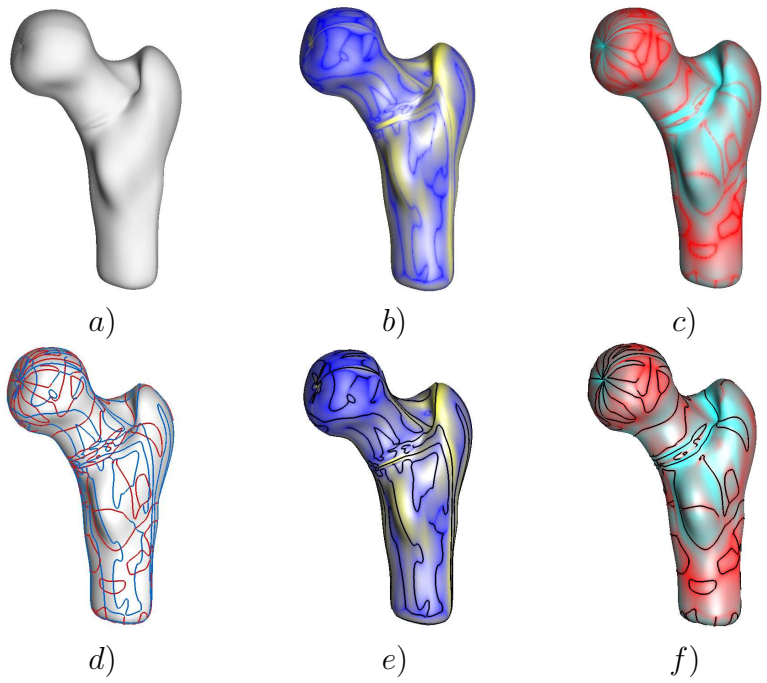

Figure 10: a) Femur bone model, b) Sampled κ_1 ridges (darker blue indicates ridge proximity), c) Sampled κ_2 ridges (brighter red indicates ridge proximity), d) Ridges overlaid on surface ($\kappa_1 \rightarrow$ blue, $\kappa_2 \rightarrow$ red), e) Traced κ_1 ridges (black) overlaid on b), f) Traced κ_2 ridges (black) overlaid on c)

Table 2: Computation Characteristics

Model	Control Mesh Size	Curvature Critical Points	Umbilics	Seed Points Time (minutes)	Ridge Tracing Time (minutes)
Bézier patch (biquartic)	5×5	23	8	0.08	0.07
Femur (biquartic)	22×21	458	12	7.03	3.68
Terrain (biquartic)	20×20	508	314	7.5	14.96

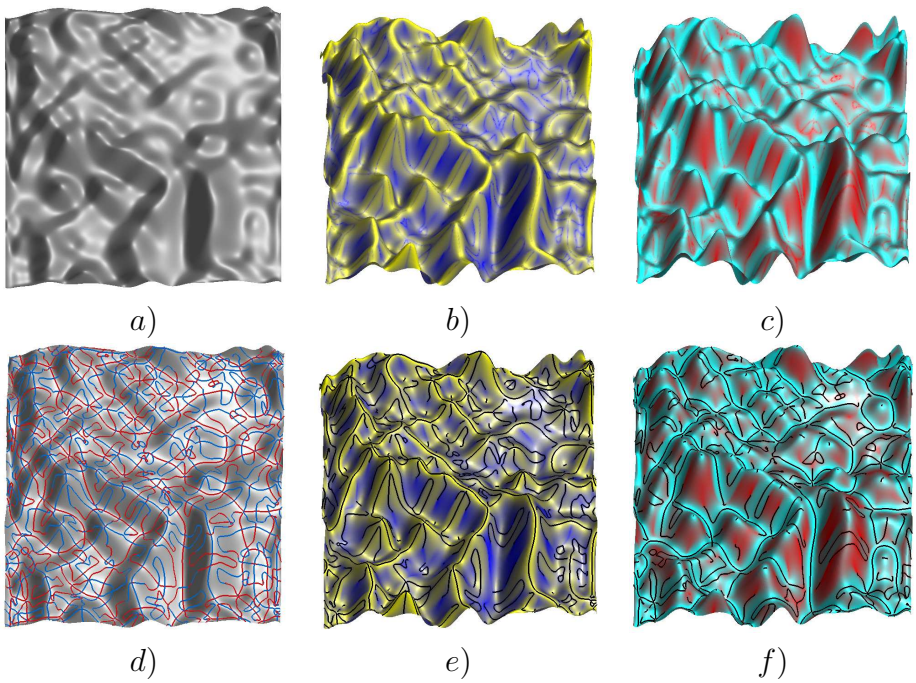

Figure 11: a) Terrain elevation model, b) Sampled κ_1 ridges (darker blue indicates ridge proximity), c) Sampled κ_2 ridges (brighter red indicates ridge proximity), d) Ridges overlaid on surface ($\kappa_1 \rightarrow$ blue, $\kappa_2 \rightarrow$ red), e) Traced κ_1 ridges (black) overlaid on b), f) Traced κ_2 ridges (black) overlaid on c)

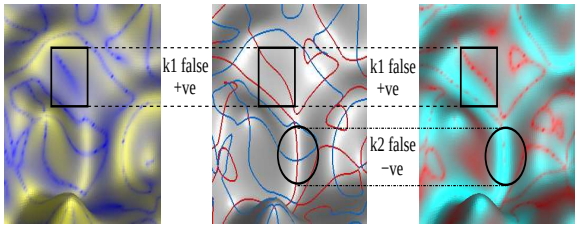

Figure 12: An example of a false positive in κ_1-ridge samples (rectangle outline) and a false negative (ellipse outline) in κ_2-ridge samples of the terrain elevation model. (a), (b) and (c) represent enlarged views of κ_1-ridge samples, traced ridges and κ_2-ridge samples of the same region of the terrain elevation model.

a type of *salient region* associated with major ridges that indicate geometrically significant regions on surfaces. First, we distinguish different types of major and secondary ridges. Second, we define the new type of salient region associated with elliptic ridges. Third, we present generic properties of boundaries of these salient regions. Fourth, we present a heuristic explanation of the nature of the regions and their relation to the elliptic ridges. Finally, we present an example of how these salient regions can be used for analyzing geometric variation.

8.1. Major and Secondary Ridges

Major Ridges. Let $\kappa_1 > \kappa_2$ denote the principal curvatures at a nonumbilic point, and let p_1, respectively p_2 denote the principal curves associated with these curvatures. Then the major ridges associated with major geometric features of the surface are curves consisting of points at which one of the following conditions is satisfied:

1. *Convex* Ridge: $\kappa_1 > \kappa_2 > 0$ such that κ_1 has a local maximum along p_1 at the point.
2. *Saddle (type I)* Ridge: $\kappa_1 > 0 > \kappa_2$ such that κ_1 has a local maximum along p_1 at the point.
3. *Saddle (type II)* Ridge: $\kappa_1 > 0 > \kappa_2$ such that κ_2 has a local minimum along p_2 at the point.
4. *Concave* Ridge: $0 > \kappa_1 > \kappa_2$ such that κ_2 has a local minimum along p_2 at the point.

All of these are types of elliptic ridges, with the convex and concave elliptic ridges occurring in regions of positive Gauss curvature and both types of saddle elliptic ridges occurring in regions of negative Gauss curvature. Also, note that the saddle elliptic ridges in the second and third cases can cross transversally. For example, in Figure 13, the convex and saddle elliptic ridges of type I are shown in cyan and the concave and saddle elliptic ridges of type II are shown in magenta.

Secondary Ridges. Secondary ridges may not correspond to perceptually obvious geometric features but provide useful insight into variation of curvature on surfaces. They are defined by one of the following conditions.

1. $\kappa_1 > \kappa_2 > 0$ with κ_1 having a local minimum along p_1
2. $\kappa_1 > 0 > \kappa_2$ with κ_1 having a local minimum along p_1.
3. $\kappa_1 > 0 > \kappa_2$ with κ_2 having a local maximum along p_2.

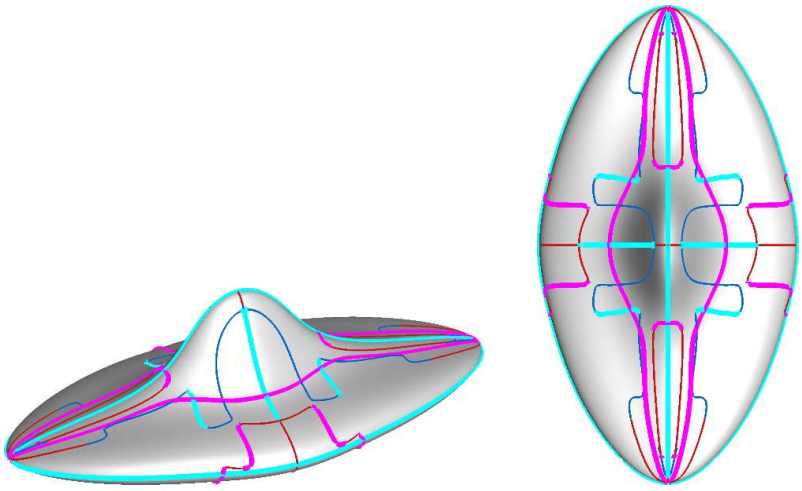

Figure 13: Major and secondary ridges of an object; a) side view, b) top view. Major ridges of κ_1 are shown in cyan and those of κ_2 are shown in magenta. Secondary ridges of κ_1 are shown in blue and those of κ_2 are shown in red.

4. $0 > \kappa_1 > \kappa_2$ with κ_2 having a local maximum along p_2.

Again in Figure 13, the secondary ridges of κ_1 are shown in blue and those of κ_2 are shown in red.

8.2. Salience Boundaries and Salient Regions

Thus far, we have divided the ridges into two distinct classes of major and secondary ridges; and for the major ridges, these are further divided into four distinct types which correspond to specific geometric features. We next further extend this analysis to associate *salient regions* surrounding the major ridges.

To define these regions, consider the partial flow along the principal curves from the major ridge points. At a major ridge point, where κ_1 has a local maximum that is not a turning point, the corresponding principal curve is transverse to the ridge. By following the principal curve away from the ridge point, eventually a point is reached where κ_1 has a local minimum that is a point on a secondary κ_1-ridge. Along the curve between these points there is a point where the function κ_1 changes from concave downward to concave upward. Since there are no intrinsic coordinates on a surface, this transition point depends upon the choice of coordinates being used. The

parameterization of the principal curve can be normalized using the unit speed parameterization. Then, in these unit speed coordinates along the principal curve, κ_1 has an inflection point on the curve between the local maximum and minimum where $t_1^T H_{\kappa_1} t_1 = 0$. There is another inflection point reached by flowing along the principal curve from the major ridge point in the negative direction. We term these inflection points the *salience boundary points* of the corresponding major ridge point and we term the flow along the principal direction from the major ridges to the salience boundary points the *salience flow*. Salience boundary points of major ridges of κ_2 are identified in a similar manner by flowing along principal curves of κ_2.

The *salience boundary for a major ridge* then is the collection of salience boundary points identified from the flow along the corresponding principal curves from the major ridges. The regions surrounding such a ridge curve and bounded by the salience boundaries defines *salient regions* associated to the major ridges. Following are the types of salience boundaries corresponding to the type of major ridges:

Types of Salience Boundaries:

1. *Convex Salience Boundary* : $\kappa_1 > \kappa_2 > 0$ and κ_1 has a first inflection point moving along p_1 from a convex elliptic ridge point in a direction of decreasing κ_1.
2. *Saddle Salience Boundary (Type I)* : $\kappa_1 > 0 > \kappa_2$ and κ_1 has a first inflection point moving along p_1 from a saddle elliptic ridge point of type I in a direction of decreasing κ_1.
3. *Saddle Salience Boundary (Type II)* : $\kappa_1 > 0 > \kappa_2$ and κ_2 has a first inflection point moving along p_2 from a saddle elliptic ridge point of type II in a direction of increasing κ_2.
4. *Concave Salience Boundary* : $0 > \kappa_1 > \kappa_2$ and κ_2 has a first inflection point moving along p_2 from a concave elliptic ridge point in a direction of increasing κ_2.

In order to compute salience boundaries and salient regions, principal curves are traced from each major ridge point on either side of the ridge using the method presented in [36]. The first inflection point on both sides, identified as the location where the sign of $t_i^T H_{\kappa_i} t_i$ changes, are marked as salience boundary points.

Salient regions and salience boundaries associated with major ridges of a surface are shown in Figure 14. For the convex and type I saddle elliptic ridges, salient regions are shown in green and for concave and type II saddle

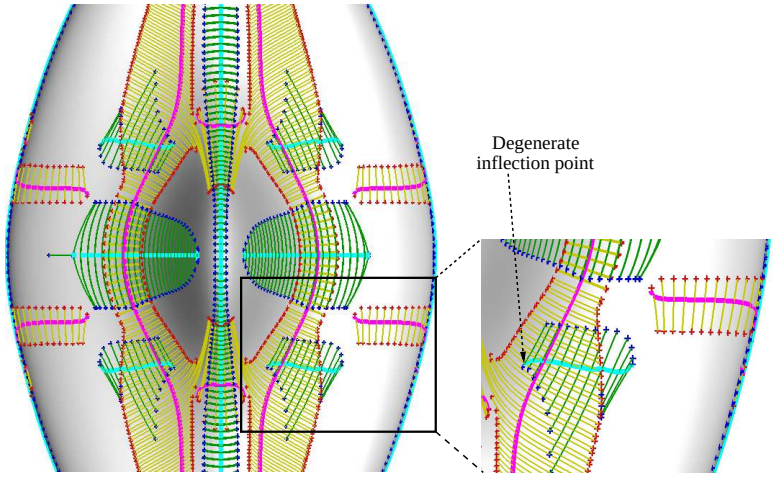

Figure 14: Salience boundaries and salient regions associated with major ridges. For κ_1, major ridges are shown in cyan, principal curve segments in salient regions are shown in green and inflection points are shown in dark blue. For κ_2, major ridges are shown in magenta, principal curve segments in salient regions are shown in yellow and inflection points are shown in dark red. Also shown is a closeup of a region that indicates a degenerate inflection point.

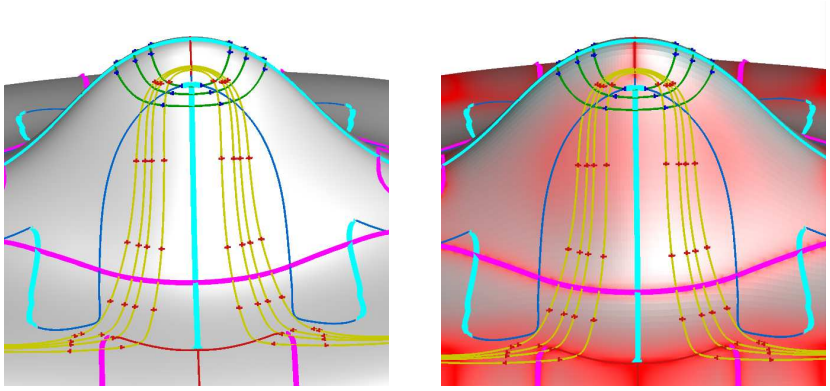

a) *b)*

Figure 15: a) Salience boundary points and other inflection points on principal curves traced from a few major ridge points. b) Results superimposed on surface indicating sampling of κ_2 ridge function. For κ_1, major ridges are shown in cyan, principal curve segments in salient regions are shown in green and inflection points are shown in dark blue. For κ_2, major ridges are shown in magenta, principal curve segments in salient regions are shown in yellow and inflection points are shown in dark red.

elliptic ridges, the salient regions are shown in yellow. It is possible for multiple inflection points to exist between a major ridge and a secondary ridge along a principal curve. In this case, the first inflection points reached by flowing from the major ridge points are treated as the salience boundary points. In Figure 15 there are other inflection points that occur on the κ_2 principal curves between the magenta and red ridges and the number of such points is consistent with the number of sign changes of $t_2^T H_{\kappa_2} t_2$ between major and secondary ridges. Note that there are no additional ridges between the additional inflection points. This is validated in Figure 15 b) where the sampled ridge condition for κ_2 is shown. In this image, the intensity of the red color is higher in the regions closer to a κ_2 ridge.

8.3. Properties of Salience Boundaries

With the exception of turning points on a ridge, the principal curve p_i corresponding to a principal curvature κ_i for that ridge is transverse to the corresponding ridge. In a small neighborhood of a non-turning point x_0, generically, the principal curvature does not have critical points at inflection points, so the implicit function theorem implies that the inflection points form a regular differentiable curve. Generically this curve is transverse to the corresponding principal curves and is disjoint from the corresponding major ridge curve except at isolated points. These properties can fail in two distinct ways at isolated points. One is when the inflection point is degenerate, and then the curve of inflection points meets the corresponding major ridge (which ends there). The other is when the curve of inflection points is tangent to the principal curve at a point disjoint from the corresponding major ridge. We describe both of these situations.

8.3.1. Salience Boundaries at Degenerate Inflection Points

For exceptional non-turning points on a ridge, the inflection point occurs at a critical point for κ_i along the principal curve. We explain the behavior at such points for the case of a convex ridge curve. The behavior of κ_1 will be modeled by the behavior of the family $g(x, u) = -x^3 + ux$. Here x is the unit speed coordinate along the principal curves, and u parameterizes the family of principal curves with the degenerate inflection point occurring at the origin. The graph of g is shown in Figure 16.

The inflection points of g, as a function of x, lie along the u axis as shown in Figure 17. For fixed $u < 0$, there are no critical points, and a single inflection point where $x = 0$. However, the direction of the salience flow is

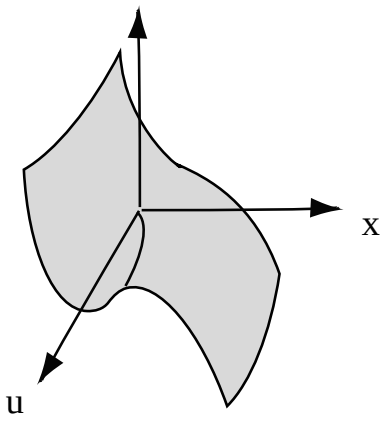

Figure 16: Graph of g illustrating degenerate inflection points

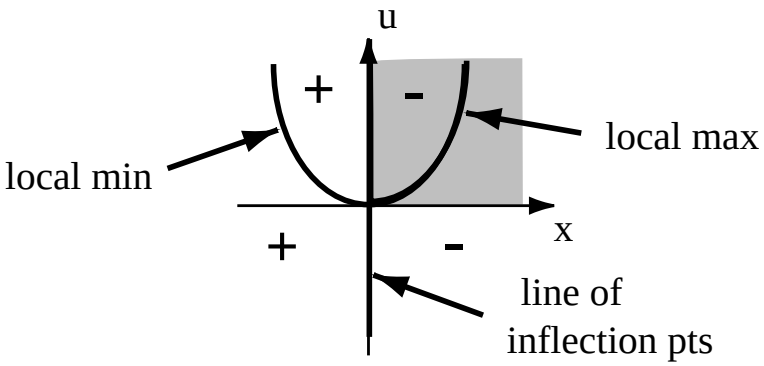

Figure 17: Decomposition of Salient Region resulting from a Degenerate Inflection Point

determined by the sign of g'' as shown in Figure 17. On each side the flow is away from the origin. At $u = 0$ the inflection point becomes degenerate and for $u > 0$ two critical points are created, one a local maximum for g $(= \kappa_1)$ which is a convex ridge point and the other a local minimum for g $(= \kappa_1)$, which is a secondary ridge. These occur on each side of 0; and the sign of g'' indicates the flow inside the parabola is toward the origin.

Hence, for this model, the positive u axis is one part of the salience boundary corresponding to the ridge formed from the local maxima with the other given by the positive x-axis representing the principal curve tangent to the curve of local maxima at the degenerate point. Then, the salient region is the shaded region. An example of a degenerate inflection point is shown

in Figure 14.

8.3.2. Salience Boundaries Tangent to Principal Curves

The second possibility is that the curve of inflection points is tangent to a principal curve at an isolated point. If we again denote κ_1 by g then this will happen at points where $g'' = 0$ (i.e., an inflection point) and $g''' = 0$ (corresponding to the principal curve being tangent to the curve of inflection points at that point). Figure 19 b) presents an example of this situation.

8.4. Properties of Salient Regions

Consider a convex elliptic ridge. Suppose the principal curvature κ_1 is large. A large curvature corresponds to a small radius of curvature. If the ridge is part of a larger region, then this high curvature can only be maintained for a short time along the corresponding principal curve. Hence, the decrease must be rapid initially which then begins to decrease more gradually. This is where an inflection point occurs. Hence, the salient region is concentrated in a small region about the major ridge curve, as illustrated in Figure 14 at the cyan ridge in the center of the image where the surface is sharply curving. If instead the curvature is much smaller, then the decrease can be more gradual so the inflection point occurs much farther along the principal curve. Then, the salient region is much larger but changes more gradually. The cyan ridges on either side of the image center of Figure 14 illustrate this behavior. Also, in Figure 15 a) the salience boundaries of κ_2 are further away from the magenta ridge since the curvature change is more gradual. An analogy here is with placing an ink pad at a point on a ridge. The sharper the change in the curvature κ_1, the smaller the region that would be marked by the ink. By contrast, if the curvature κ_1 changes more gradually, a much larger region will be marked by the ink. The salient region is similar to such a marked region.

8.5. Analyzing Geometric Variation using Salient Regions

Salient regions are an effective visualization tool for analyzing higher order geometric properties of surfaces and can also be used to measure geometric variation of similar objects. Salient regions are especially useful in distinguishing geometric properties of a population of similar objects when ridges on the surfaces occur at similar locations. Figure 18 shows front and back views of an object that is slightly asymmetric. The major and secondary ridges are slightly different on the front and back sides of the model but do

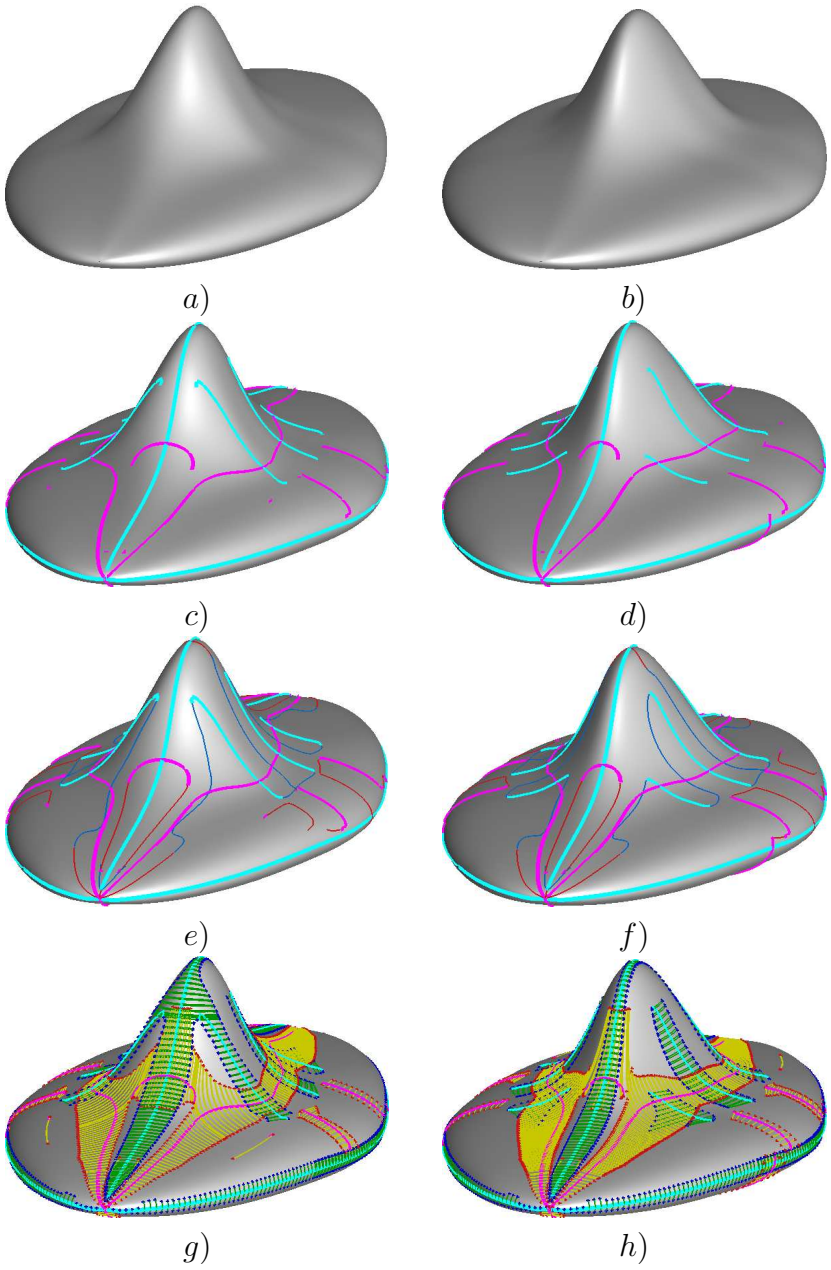

Figure 18: Visualizing geometric differences using salient regions. a) front view and, b) back view of a slightly asymmetric object, c) and d) major ridges only, e) and f) all ridges, g) and h) salient regions.

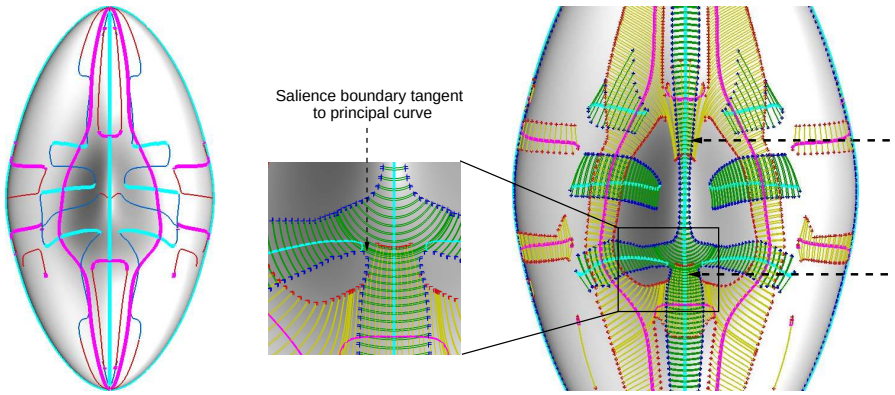

Figure 19: Visualizing geometric differences using salient regions. a) the major ridge corresponding to the bump in the surface lies in the center on both asymmetric regions, other major ridges are slightly different across plane of symmetry, b) salient regions clearly indicate geometric differences in the asymmetric regions pointed by the arrows. Also shown is a close up view of a region that contains a point where the salience boundary is tangent to the principal curve.

not clearly distinguish the differences. In particular, the major ridge running along the bump of the model is almost identical on both sides. In this case the salient regions clearly indicate the geometric differences and enable quantitative evaluation of the differences. The differences are clearly visible from the top view of the object as shown in Figure 19.

9. Conclusions

Ridges are important feature curves and have a wide variety of applications. Umbilics and therefore, ridges around umbilics, also represent important aspects of the shape of a surface. Ridges exhibit complex behavior around umbilics. This paper presents a new algorithm for numerically tracing ridges on B-Spline surfaces that has been designed using generic properties of ridges. In addition, a new type of geometrically salient region corresponding to major ridges is defined.

The tracing algorithm involves traversing curvature lines in a novel manner and accurately captures the behavior of ridges at all points on a surface including umbilics. The technique takes into account turning points without directly computing them, thereby allowing ridge computation on C^3 models, instead of requiring C^4 smoothness. Our technique has been designed for

rational tensor product B-Spline surface representations. Since ridge computation is local to a tensor product patch, it is directly extensible for models with multiple patches. Some special cases, such as ridges parallel to a domain boundary, may need to be addressed. Trimmed freeform surfaces also may be addressed by minor modifications to the algorithm. The algorithm design enables optimization using parallel processing techniques, which would further improve computation time. The approach can be further extended to surfaces with isolated irregular points. We plan to pursue these modifications in future work. The technique presented in this paper avoids errors in ridge computation associated with sampling-based approaches, while at the same time, it can generate results for complex models that were previously computationally intractable. The result is a set of trace segments that are available for other applications, such as surface segmentation, matching, quality control and visualization.

We identify elliptic ridges as major ridges with geometric significance. These ridges supplemented with salient regions are very useful for studying geometric variation across a population of similar objects. Earlier methods for computing significance of ridges only account for geometric properties of surfaces only at the ridge points. The type of salient region presented in this paper provides a new method of quantifying geometric importance of ridges that also takes into account salient neighborhoods of ridges. We are currently investigating several measures based on salient regions to precisely quantify geometric properties of surfaces at and in the neighborhood of ridges.

10. Acknowledgements

This work was supported in part by NSF (CCF0541402), NSF DMS-0706941, the Basic Science Research Program through the National Research Foundation of Korea (NRF) funded by the Ministry of Education, Science and Technology (2010-0028631), and the Korea Science and Engineering Foundation (KOSEF) grant funded by the Korea government (MEST) (2010-0015879). All opinions, findings, conclusions or recommendations expressed in this document are those of the authors and do not necessarily reflect the views of the sponsoring agencies.

[1] I. Porteous, The normal singularities of a submanifold, Journal of Differential Geometry 5 (1971) 543–564.

[2] J. Koenderink, Solid shape, MIT Press Cambridge, MA, USA, 1990.

[3] A. Guéziec, Large deformable splines, crest lines and matching, in: Computer Vision, 1993. Proceedings., Fourth International Conference on, 1993, pp. 650–657.

[4] J. Kent, K. Mardia, J. West, Ridge curves and shape analysis, in: The British Machine Vision Conference 1996, 1996, pp. 43–52.

[5] X. Pennec, N. Ayache, J.-P. Thirion, Landmark-based registration using features identified through differential geometry, in: I. Bankman (Ed.), Handbook of Medical Image Processing and Analysis - New edition, Academic Press, 2008, Ch. 34, pp. 565–578.

[6] G. Subsol, Crest lines for curve-based warping, Brain Warping (1999) 241–262.

[7] F. Cole, A. Golovinskiy, A. Limpaecher, H. S. Barros, A. Finkelstein, T. Funkhouser, S. Rusinkiewicz, Where do people draw lines?, ACM Transactions on Graphics (Proc. SIGGRAPH) 27 (3).

[8] V. Interrante, H. Fuchs, S. Pizer, Enhancing transparent skin surfaces with ridge and valley lines, in: Proceedings of the 6th conference on Visualization'95, IEEE Computer Society Washington, DC, USA, 1995.

[9] K. Ma, V. Interrante, Extracting feature lines from 3D unstructured grids, in: Visualization'97., Proceedings, 1997, pp. 285–292.

[10] M. Hosaka, Modeling of curves and surfaces in CAD/CAM with 90 figures Symbolic computation, Springer, 1992.

[11] J. Little, P. Shi, Structural lines, TINs, and DEMs, Algorithmica 30 (2) (2001) 243–263.

[12] T. Tasdizen, R. Whitaker, Feature preserving variational smoothing of terrain data, in: Proceedings of the Second IEEE Workshop on Variational, Geometric and Level Set Methods in Computer Vision (VLSM'03)(Institute of Electrical and Electronics Engineers, 2003), pp. 121–128.

[13] K. Ko, T. Maekawa, N. Patrikalakis, H. Masuda, F. Wolter, Shape intrinsic fingerprints for free-form object matching, in: Proceedings of the eighth ACM symposium on Solid modeling and applications, ACM New York, NY, USA, 2003, pp. 196–207.

[14] N. Patrikalakis, T. Maekawa, Shape interrogation for computer aided design and manufacturing, Springer, 2002.

[15] F. Cazals, M. Pouget, Topology driven algorithms for ridge extraction on meshesINRIA Technical Report.

[16] Y. Ohtake, A. Belyaev, H. Seidel, Ridge-valley lines on meshes via implicit surface fitting, ACM Transactions on Graphics 23 (3) (2004) 609–612.

[17] S. Yoshizawa, A. Belyaev, H. Yokota, H. Seidel, Fast and faithful geometric algorithm for detecting crest lines on meshes, in: Computer Graphics and Applications, 2007. PG'07. 15th Pacific Conference on, 2007, pp. 231–237.

[18] F. Cazals, J. Faugère, M. Pouget, F. Rouillier, The implicit structure of ridges of a smooth parametric surface, Computer Aided Geometric Design 23 (7) (2006) 582–598.

[19] I. Porteous, Geometric differentiation: for the intelligence of curves and surfaces, Cambridge University Press, 2001.

[20] P. Hallinan, G. Gordon, A. Yuille, P. Giblin, D. Mumford, Two-and three-dimensional patterns of the face, AK Peters, Ltd. Natick, MA, USA, 1999.

[21] F. Cazals, J. Faugère, M. Pouget, F. Rouillier, Topologically certified approximation of umbilics and ridges on polynomial parametric surfaceINRIA Technical Report.

[22] F. Cazals, J. Faugère, M. Pouget, F. Rouillier, Ridges and umbilics of polynomial parametric surfaces, Geometric Modeling and Algebraic Geometry (2007) 141–159Jüttler, B. and Piene, R. (eds.).

[23] M. Jefferies, Extracting Crest Lines from B-spline Surfaces, Arizona State University, 2002.

[24] R. Morris, Symmetry of Curves and the Geometry of Surfaces, Ph.D. thesis, PhD thesis, University of Liverpool (1990).

[25] K. Hildebrandt, K. Polthier, M. Wardetzky, Smooth feature lines on surface meshes, in: Symposium on geometry processing, 2005, pp. 85–90.

[26] S. Kim, C. Kim, Finding ridges and valleys in a discrete surface using a modified MLS approximation, Computer-Aided Design 37 (14) (2005) 1533–1542.

[27] G. Stylianou, G. Farin, Crest lines extraction from 3D triangulated meshes, Hierarchical and geometrical methods in scientific visualization (2003) 269–281.

[28] A. Belyaev, Y. Ohtake, K. Abe, Detection of ridges and ravines on range images and triangular meshes, in: Proceedings of SPIE, Vol. 4117, 2000, p. 146.

[29] Y. Lai, Q. Zhou, S. Hu, J. Wallner, H. Pottmann, Robust feature classification and editing, IEEE Transactions on Visualization and Computer Graphics 13 (1) (2007) 34–45.

[30] A. Belyaev, A. Pasko, T. Kunii, Ridges and ravines on implicit surfaces, in: Computer Graphics International, 1998. Proceedings, 1998, pp. 530–535.

[31] I. Bogaevski, V. Lang, A. Belyaev, T. Kunii, Color ridges on implicit polynomial surfaces, GraphiCon 2003, Moscow, Russia.

[32] J. Thirion, A. Gourdon, The 3D marching lines algorithm and its application to crest lines extraction.

[33] O. Monga, S. Benayoun, Using partial derivatives of 3D images to extract typical surface features, Computer Vision and Image Understanding 61 (2) (1995) 171–189.

[34] E. Cohen, R. Riesenfeld, G. Elber, Geometric modeling with splines: an introduction, AK Peters, Ltd., 2001.

[35] B. O'Neill, Elementary differential geometry, 2nd Edition, Academic press, 2006.

[36] T. Maekawa, F. Wolter, N. Patrikalakis, Umbilics and lines of curvature for shape interrogation, Computer Aided Geometric Design 13 (2) (1996) 133–161.

[37] T. Maekawa, N. Patrikalakis, Interrogation of differential geometry properties for design and manufacture, The Visual Computer 10 (4) (1994) 216–237.

[38] G. Elber, M. Kim, Geometric constraint solver using multivariate rational spline functions, in: Proceedings of the sixth ACM symposium on Solid modeling and applications, ACM New York, NY, USA, 2001, pp. 1–10.

[39] G. Elber, T. Grandine, Efficient solution to systems of multivariate polynomials using expression trees, in: IEEE International Conference on Shape Modeling and Applications, 2008. SMI 2008, 2008, pp. 163–169.

[40] D. Johnson, E. Cohen, An improved method for haptic tracing of sculptured surfaces, in: Symp. on Haptic Interfaces, ASME International Mechanical Engineering Congress and Exposition, Anaheim, CA, 1998.

[41] X. Liu, L. Yang, J. Yong, H. Gu, J. Sun, A torus patch approximation approach for point projection on surfaces, Computer Aided Geometric Design 26 (5) (2009) 593–598.

[42] G. Elber. The IRIT modeling environment, version 10.0 [online] (2008).

[43] D. Hastings, P. Dunbar, G. Elphingstone, M. Bootz, H. Murakami, H. Maruyama, H. Masaharu, P. Holland, J. Payne, N. Bryant, et al., The global land one-kilometer base elevation (GLOBE) digital elevation model. Version 1.0. National Oceanic and Atmospheric Administration, National Geophysical Data Center, Boulder, Colorado, National Geophysical Data Center, Digital data base on the World Wide Web (URL: http://www.ngdc.noaa.gov/mgg/topo/globe.html) and CD-ROMs.

[44] S. Musuvathy, E. Cohen, Extracting Principal Curvature Ridges from B-Spline Surfaces with Deficient Smoothness, Advances in Visual Computing (2009) 101–110.